BULLETIN OF THE POLISH ACADEMY OF SCIENCES
TECHNICAL SCIENCES
DOI: 10.24425/bpasts.2026.158310

Application of Eurocode 2, ACI and RILEM Model in Predicting Shrinkage of 3D-Printed Concretes: Challenges and Model Optimization

Karol Federowicz[1*], Marcin Hoffmann [2], Nikola Tošić[3], Pawel Sikora[1]

[1] Faculty of Civil and Environmental Engineering, West Pomeranian University of Technology in Szczecin, Poland
[2] Faculty of Mechanical Engineering and Mechatronics, West Pomeranian University of Technology in Szczecin, Poland
[3] Civil and Environmental Engineering Department, Universitat Politècnica de Catalunya, Barcelona, Spain

Abstract. 3D-printed concrete (3DPC) cures under non-standard conditions due to the absence of formwork and external curing, which leads to rapid moisture evaporation. Combined with a unique mix design—characterized by high binder content and reduced water-to-cement ratio—this results in significantly different shrinkage behavior compared to conventional concrete, particularly at early ages. Measuring shrinkage in 3D-printed elements is technically challenging and often technically challenging, which emphasizes the need for reliable predictive models. Since well-established models exist for traditional concrete, this study focuses on estimating updated coefficient values for three widely used models—Eurocode 2 (EC2), RILEM B4, and ACI 209-92—to enable their application to 3DPC. Experimental shrinkage measurements were performed on multi-layer printed specimens consisting of six layers, each with a 40×10 mm cross-section and a total length of 500 mm. Both non-contact laser sensors and LVDT devices were used. Model parameters were estimated using nonlinear regression techniques. The results show that all three models can accurately describe the shrinkage behavior of 3DPC after recalibration, with coefficients of determination exceeding 0.94. This confirms the potential of adapting existing shrinkage models—originally developed for conventional concrete—to the specific characteristics of 3D-printed materials.

Keywords: 3D printed concrete, shrinkage prediction, Eurocode 2 model, ACI 209, RILEM B4

1. INTRODUCTION

3D printing using cementitious mixtures is currently one of the most rapidly developing fields in concrete technology [1–3]. This technology can improve safety on construction sites, economic efficiency and freedom of design [4,5]. Additive manufacturing enables greater freedom in shaping geometries, eliminates the need for traditional formwork, and automates the construction process. Despite its numerous advantages, this technology has challenges that must be addressed, including the development of appropriate reinforcement strategies and the establishment of effective curing methodologies during the hardening phase[6–8].

The elimination of formwork from the technological process and the lack of traditional external curing methods result in significant moisture evaporation from the concrete. The loss of free water from the mixture leads to drying shrinkage. The necessity of studying and analyzing shrinkage in 3D-printed concretes has been emphasized by numerous researchers e.g. Federowicz et al. [9].

Using digital image correlation (DIC) techniques, Moelich et al. [10] investigated shrinkage deformations in a multi-layered printed element. After 40 minutes from printing, the surface was sufficiently dry to allow the application of paint and the preparation of an appropriate pattern. Deformations were recorded over the following 3 h. During this period, the upper layers exhibited free shrinkage of approximately 2400 μm/m and up to 1400 μm/m under laboratory conditions and under reduced relative humidity conditions, respectively.

Van Der Putten et al. [11] also researched shrinkage in 3D-printed concrete elements. Using the DIC method and the GOM Correlate software, they recorded the deformations of a cementitious composite composed of cement, sand, and water, with a water-to-cement ratio (w/c) of 0.36. After 24 h of curing, the specimens exhibited approximately 1500 μm/m deformations, increasing to around 3500 μm/m after 5 days.

Zhang and Xiao [12] investigated shrinkage in nine-layer 3D-printed specimens. The samples were not subjected to curing procedures, and deformation measurements commenced immediately after printing. Similarly, the DIC method was applied, embedding specialized reference points into the fresh mixture. The maximum recorded deformation for a mixture of cement and sand in a 1:1 ratio, with a w/c ratio of 0.35, reached 4000 μm/m after 3 h of testing.

Markin and Mechtcherine [13] also implemented the 2D DIC method to record deformations of 3D-printed concrete. This approach required a time-consuming calibration procedure before each measurement. The total recorded free shrinkage exceeded -9000 μm/m after 3 h. It is worth mentioning that,

*e-mail: karol.federowicz@zut.edu.pl

prior to measurement, samples were sprayed with paint to create the black-and-white pattern required for DIC.

An alternative to digital image analysis may be the use of fiber optic sensors. One of the first studies on this subject was presented by Zhang et al. [14], who fabricated multilayer specimens with embedded sensors placed in the interfacial zones. During the first few hours of measurement, the sensors recorded plastic shrinkage at a level of 1200 µm/m.

Due to technical challenges associated with measuring shrinkage in printed elements, some researchers opt to use standard measurement methods. Shahmirzadi et al. [15] conducted tests based on the EN 12617-4 standard [16], obtaining strains of approximately 1600 µm/m after 28 days, which noticeably deviates from the values measured using DIC. Le et al. [17] also investigated shrinkage on specimens with dimensions of 75×75×229 mm, recording over 700 µm/m after 28 days.

A significant challenge in measuring the total shrinkage of 3D-printed concrete elements is the need to employ advanced measurement techniques based on digital image analysis or distributed optic fiber sensors (DOFS). Therefore, researchers are exploring the possibility of analytically determining the shrinkage of printed mixtures using empirical formulas, drawing analogies from existing shrinkage prediction models developed for conventional concrete, as suggested by Federowicz [18].

Some researchers, such as Ma et al. [19], attempted to develop completely novel analytical models. Deriving such models is highly labor-intensive and requires extensive measurements across multiple mixtures to obtain reliable data. However, even large-scale studies typically achieve only around 20% accuracy.

An alternative approach involves optimizing existing numerical models initially developed for conventional concrete. One of the most frequently used models, referenced in European standards, is the Eurocode 2 model, described in EN 1992-1-1:2004 [20](referred to as Eurocode 2 or EC2). This model is based on the FIB Model Code 1990, which represents a modified version of the first 1978 model proposed by the Euro-International Committee for Concrete (CEB) and the International Federation for Prestressing (FIP), now operating under the *fib* organization. In the case of high-strength concretes, the B4 model [21], proposed and published by RILEM TC-242-MDC is frequently used in research. Globally, the ACI 209-92 model [22] is also widely adopted as an alternative to the European standard.

Despite the growing body of work on shrinkage in printable cementitious materials, reported results remain difficult to compare directly because they depend strongly on the measurement technique (e.g., DIC, optical sensors, standardized linear shrinkage tests), specimen geometry, and exposure conditions. Consequently, there is a clear need for practical approaches that enable the use of well-established shrinkage models while accounting for the specific early-age behavior and boundary conditions of 3D-printed elements.

This paper compares shrinkage measurements in 3D-printed concrete elements with predicted values based on the Eurocode 2, B4 and ACI 209-92 model. These models were deliberately chosen to represent different geographic regions and varying levels of complexity — ACI being the simplest, followed by the standardized Eurocode 2, and then the highly advanced B4 model. Additionally, an attempt is made to optimize the model's parameters for more accurate shrinkage predictions in 3D-printed concrete. It is also worth noting the existence of the B4s model, a simplified, design-oriented version of B4 that requires fewer input parameters and relies mainly on compressive strength; however, this model was not included in the present analysis.

2. MATERIALS AND METHODS

The reference mixture was a 3D-printed concrete with a binder composed of CEM I 42.5R cement, fly ash, and silica fume. Additionally, natural sand (<2 mm), water, and a superplasticizer were used to achieve the desired consistency. The designed concrete mixture had a water-to-cement ratio (*w/c*) of 0.35, a water-to-binder ratio (*w/b*) of approximately 0.24, and an aggregate-to-cement ratio (*a/c*) of approximately 2.04. The mixture was thoroughly analyzed in terms of its rheological properties in a previous publication of Federowicz et al. [9]. The composition of the mixture is presented in Table 1.

TABLE 1. 3D printed concrete mixture composition [kg/m^3].

Cement	Fly Ash	Silica Fume	Fine sand	Superplasticizer	Water
600	180	90	1225	2.70	210

Fig. 1. Samples preparation: 3D printer (left); sample during printing process (right).

2.1. Shrinkage measurement

The shrinkage test specimens were printed using a Cartesian robot with parameters specified by Sikora et al. [23]. A rectangular nozzle with a 40×10 mm cross-section and a 45° outlet angle was used to print six-layer specimens, simulating the structure of a multi-layered wall. A photograph of the specimens during the printing process is shown in Fig. 1.

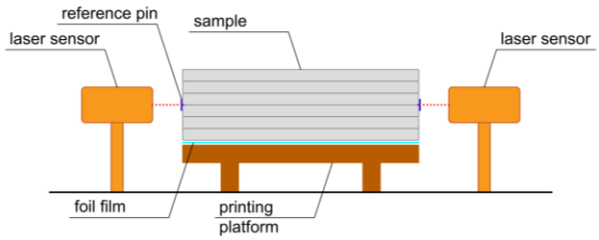

Fig. 2. Schematic drawing of the shrinkage measuring setup.

The shrinkage measurements were conducted using a specially designed and constructed measurement setup. The core of the measurement system was a non-contact optical measurement method utilizing laser displacement sensors (OMRON ZX1-LD50). These sensors have a measurement accuracy of 2 µm and continuously recorded deformations at a sampling rate of 0.02 Hz. Schematic drawing representing measuring setup is presented in Fig. 2.

As a control, the deformations of one specimen were additionally monitored using LVDT sensors and a specially designed holder, which was embedded in the specimen during printing. The measurement setup is shown in Fig. 3.

2.2. Shrinkage prediction models.

The Eurocode 2 (EC2) shrinkage prediction model was first applied in this study. According to its assumptions, the model can be applied to all types of concrete within EC2 strength classes under thermal-humidity conditions.

In the EC2 analytical model, the total shrinkage-induced deformation of concrete should be determined using Eq. (1):

$$\varepsilon_{cs} = \varepsilon_{cd} + \varepsilon_{ca} \qquad (1)$$

where:

ε_c – total shrinkage strain,

ε_{cd} – drying shrinkage strain,

ε_{ca} – autogenous shrinkage strain.

Drying shrinkage deformations as a function of time are given by Equation (2):

$$\varepsilon_{cd}(t) = \varepsilon_{cd,0} \cdot \beta_{ds}(t, t_s) \cdot k_h \qquad (2)$$

in which:

$$\varepsilon_{cd,0} = 0{,}85 \cdot (220 + 110 \cdot \alpha_{ds1}) \cdot exp\left(-\alpha_{ds2} \cdot \frac{f_{cm}}{f_{cm0}}\right) \cdot \beta_{RH} \qquad (3)$$

$$\beta_{RH} = 1{,}55 \cdot \left[1 - \left(\frac{RH}{RH_0}\right)^3\right] \qquad (4)$$

where:

$\varepsilon_{cd,0}$ – nominal value of drying shrinkage determined from Eq. (3) in µm⁄m,

$\beta_{ds}(t,t_s)$ – time-dependent shape coefficient

k_h - coefficient dependent on the characteristic cross-sectional dimension.

α_{ds1} – coefficient dependent on the type of cement, for class R α_{ds1}=6,

α_{ds2} – coefficient dependent on the type of cement, for class R α_{ds2}=0.11,

f_{cm} – average compressive strength of concrete in MPa,

f_{cm0} – reference value equal to 10 MPa,

β_{RH} – relative humidity coefficient

RH – relative humidity of the environment in %,

RH_0 – reference value equal to 100%.

$$\beta_{ds}(t, t_s) = \frac{(t - t_s)}{t - t_s + 0{,}04\sqrt{h_0{}^3}} \qquad (5)$$

where:

t – age of the concrete at the considered moment in days,

t_s – age of the concrete at the start of the drying process in days,

h_0 – characteristic cross-sectional dimension equal to $2A_c/u$,

A_c – cross-sectional area of the element in mm2,

u – perimeter of the cross-section exposed to drying in mm.

Autogenous shrinkage strain is given by Eq. (6):

$$\varepsilon_{ca}(t) = \varepsilon_{ca}(\infty) \cdot \beta_{as}(t) \qquad (6)$$

$$\varepsilon_{ca}(\infty) = 2{,}5 \cdot (f_{ck} - 10) \qquad (7)$$

$$\beta_{as}(t) = 1 - exp(-0{,}2 \cdot t^{0{,}5}) \qquad (8)$$

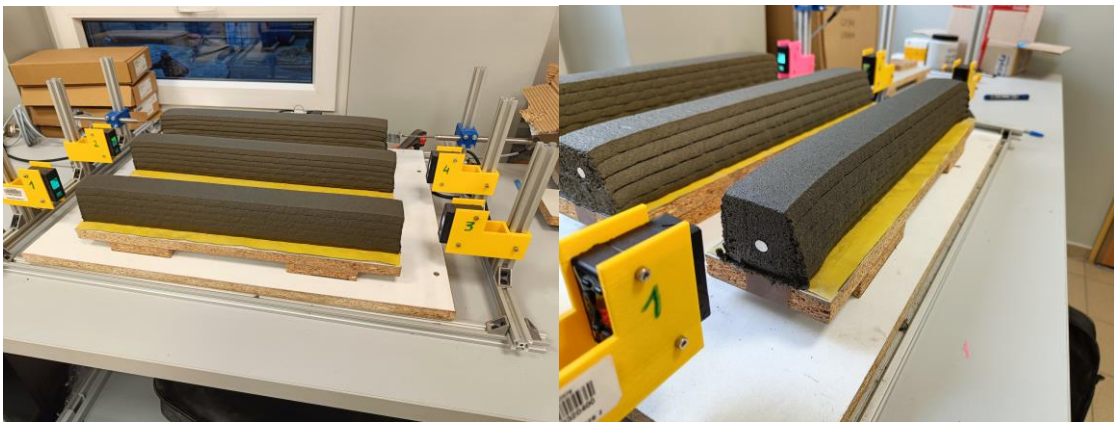

Fig. 3. Measuring shrinkage of 3D printed samples: measuring setup (left); sample with a reference point for laser measurement (right).

where:
$\varepsilon_{ca}(\infty)$ – nominal value of autogenous shrinkage in μm/m
$\beta_{as}(t)$ – time-dependent shape coefficient
f_{ck} – f_{cm}-8 MPa where f_{cm} is mean compressive strength,
t – age of concrete in a given time in days.
The B4 model, recommended by the RILEM organization, has minor limitations when used to estimate total shrinkage. The concrete should have a compressive strength, determined at 28 days on cylindrical specimens, in the range of 15 to 70 MPa. Additionally, the cement content should be between 200 and 1500 kg/m³, *w/c* ranged 0.22 to 0.87 and *a/c* between 1.0 and 13.2. Importantly, the model authors allow its application to mixtures that fall outside these boundary conditions, while noting that this may negatively affect prediction accuracy. In the analytical model recommended by RILEM, the total strain of concrete should be determined according to the following Eq. (9):

$$\epsilon(t) = (t,t') \cdot \sigma + \epsilon_{sh}(t,t_0) + \epsilon_{au}(t,t_0) + \alpha_T \Delta T(t) \quad (9)$$

Since the printed specimens were not subjected to any external load during the measurements (σ = 0), and a constant temperature was maintained stable (Δ*T*(t) = 0), Eq. (9) takes the following form:

$$\epsilon(t) = \epsilon_{sh}(t,t_0) + \epsilon_{au}(t,t_0) \quad (10)$$

where:
$\epsilon(t)$ – total shrinkage,
$\epsilon_{sh}(t,t_0)$ – drying shrinkage at time t,
$\epsilon_{au}(t,t_0)$ – autogenous shrinkage at time t,
Drying shrinkage in the analyzed model should be determined according to the following Eq. (11):

$$\epsilon_{sh}(t,t_0) = \epsilon_{sh,\infty}(t_0) \cdot k_h \cdot \tanh\left(\frac{t-t_0}{\tau_{sh}}\right)^p \quad (11)$$

where:
$\epsilon_{sh,\infty}(t_0)$ – final drying shrinkage,
k_h – relative humidity factor,
p – fixed coefficient equal 0.5,
t – concrete age in days,
t_0 – concrete age in days at the beginning of drying,
τ_{sh} – shrinkage half-time.
Since the printed specimens were exposed to drying from the very beginning, t_0=0. The relative humidity coefficient should be determined according to the following Eq. (12):

$$k_h = \begin{cases} 1-h^3 & h \le 0.98 \\ -0{,}2 & \text{for } h = 1 \\ 12.94(1-h) - 0.2 & 0.98 \le h \le 1.0 \end{cases} \quad (12)$$

where:
h – relative humidity of air [-].
The coefficient τ_{sh} accounts for the influence of the mixture composition and the specimen geometry on drying shrinkage, in accordance with the following Eq. (13):

$$\tau_{sh} = \tau_0 \cdot k_{\tau a} \cdot \left(k_s \cdot \frac{D}{1\text{mm}}\right)^2 \quad (13)$$

where:
τ_0 – the coefficient of the basic drying shrinkage value is defined by the following equation (14),
$k_{\tau a}$ – coefficient dependent on the type of aggregate,
k_s – shape coefficient, for prismatic specimens $k_s = 1{,}25$,
D – effective size of the specimen.

$$\tau_0 = \tau_{cem} \cdot \left(\frac{a/c}{6}\right)^{p_{\tau a}} \cdot \left(\frac{w/c}{0{,}38}\right)^{p_{\tau w}} \cdot \left(\frac{6{,}5c}{\rho}\right)^{p_{\tau c}} \quad (14)$$

where:
$\tau_{cem}, p_{\tau a}, p_{\tau w}, p_{\tau c}$ – coefficients dependent on the type of cement used,
a – aggregate content in the mix, in kg/m³,
c – cement content in the mix, in kg/m³,
w – water content in the mix, in kg/m³,
ρ – bulk density of concrete in kg/m³.
The final drying shrinkage, $\varepsilon_{sh,\infty}(t_0)$, taking into account the effect of aging on elastic stiffness, should be determined using the following Eq. (15):

$$\epsilon_{sh,\infty}(t_0) = -\epsilon_0 k_{\epsilon a} \cdot \frac{E(7\beta_{Th}+600\beta_{Ts})}{E(t_0+\tau_{sh}\cdot\beta_{Ts})} \quad (15)$$

where:
ϵ_0 – basic shrinkage value,
$k_{\epsilon a}$ – aggregate factor, for natural sand $k_{\epsilon a} = 0{,}71$,
β_{Th}, β_{Ts} – correction coefficients accounting for ambient temperature variation, in presented tests $\beta_{Th} = \beta_{Ts} = 1$,
$E(t)$ – modulus of elasticity of concrete at ***t*** days, calculated as $E(28) \cdot \left(\frac{t}{4+0{,}85t}\right)^{0{,}5}$.
The basic shrinkage value can be determined using the following Eq. (16):

$$\epsilon_0 = \epsilon_{cem} \cdot \left(\frac{a/c}{6}\right)^{p_{\epsilon a}} \cdot \left(\frac{w/c}{0{,}38}\right)^{p_{\epsilon w}} \cdot \left(\frac{6{,}5c}{\rho}\right)^{p_{\epsilon c}} \quad (16)$$

where:
$\epsilon_{cem}, p_{\epsilon a}, p_{\epsilon w}, p_{\epsilon c}$ – coefficients dependent on the type of cement used.
Autogenous shrinkage in the B4 model should be determined according to the following Eq. (17):

$$\epsilon_{au}(t,t_0) = \epsilon_{au\infty} \cdot \left[1 + \left(\frac{\tau_{au}}{t+t_0}\right)^{\alpha}\right]^{r_t} \quad (17)$$

where:
$\epsilon_{au\infty}$ – final autogenous shrinkage,
τ_{au} – autogenous shrinkage halftime $\tau_{au} = \tau_{au,cem} \cdot \left(\frac{w/c}{0{,}38}\right)^{r_{\tau w}}$,
$\tau_{au,cem}, r_{\tau w}$ – coefficients dependent on the type of cement used.
α – auxiliary parameter $\alpha = r_\alpha \cdot \left(\frac{w/c}{0{,}38}\right)$,
r_α, r_t – coefficients dependent on the type of cement used, $r_\alpha = 1{,}4$ and $r_t - 4{,}5$.
The final autogenous shrinkage can be determined according to the following Eq. (18):

$$\epsilon_{au\infty} = \epsilon_{au,cem} \cdot \left(\frac{a/c}{6}\right)^{r_{\epsilon a}} \cdot \left(\frac{w/c}{0{,}38}\right)^{r_{\epsilon w}} \quad (18)$$

where:
$\epsilon_{au,cem}, r_{\epsilon a}, r_{\epsilon w}$ – coefficients dependent on the type of cement used.
The ACI 209-92 model (ACI92) is widely used in North American and Asian countries. Its main advantages are the simplicity of calculations, the minimal amount of required input data, and its broad applicability. Its limitations are related to the cement content (between 279 kg/m³ and 446 kg/m³), the ambient relative humidity (above 40%), the type of cement used (type N or R), and a minimum curing period of 24 hours, similarly to EC2. Additionally, the ACI model estimates shrinkage exclusively as a total strain, without distinguishing between drying and autogenous components,

which limits its ability to reflect the complex early-age mechanisms governing shrinkage in 3D-printed concrete. Another important limitation is that the influence of specimen geometry is incorporated through a simplified surface-area-to-volume ratio, which was originally calibrated for conventional cast specimens and does not adequately capture the highly exposed and slender geometries typical of additively manufactured elements. Moreover, although the model formulation includes several correction factors, many of them are recommended to be taken as equal to unity in practical applications, which further restricts the model's flexibility when applied outside its original range of validity. For the investigated printing mix, three out of the four main assumptions are not met, which inevitably affects the predictions. Nevertheless, the model was included in the analyses to quantify the extent of mismatch of the unmodified formulation and to assess the effectiveness of the parameter recalibration for this case.

In the analytical model recommended by the ACI organization, the total shrinkage-induced strain of concrete should be determined according to the following Eq. (19):

$$\varepsilon_{\mathrm{sh}}(t,t_{\mathrm{c}}) = \frac{(t-t_{\mathrm{c}})^{\alpha}}{f+(t-t_{\mathrm{c}})^{\alpha}} \cdot \varepsilon_{\mathrm{shu}} \quad (19)$$

where:

$\varepsilon_{\mathrm{sh}}(t,t_{\mathrm{c}})$ – total concrete shrinkage,

t – concrete age,

t_{c} – concrete age at the onset of drying,

α – specimen size coefficient, recommended value $\alpha = 1{,}0$,

f – specimen shape coefficient,

$\varepsilon_{\mathrm{shu}}$ – final concrete shrinkage.

The specimen shape coefficient f, when using the SI metric system, should be determined according to the following Eq. (20):

$$f = 26 \cdot exp\left(1{,}42 \cdot 10^{-2} \cdot \left(\frac{V}{S}\right)\right) \quad (20)$$

where:

V – sample volume,

S – drying surface of the sample.

The final shrinkage value $\varepsilon_{\mathrm{shu}}$ should be determined according to the following Eq. (21):

$$\varepsilon_{\mathrm{shu}} = 780 \cdot \gamma_{\mathrm{sh}} \cdot 10^{-6} \quad (21)$$

where:

γ_{sh} – the combined correction coefficient determined according to the following Eq. (22).

$$\gamma_{\mathrm{sh}} = \gamma_{\mathrm{sh,tc}} \cdot \gamma_{\mathrm{sh,RH}} \cdot \gamma_{\mathrm{sh,vs}} \cdot \gamma_{\mathrm{sh,s}} \cdot \gamma_{\mathrm{sh,\psi}} \cdot \gamma_{\mathrm{sh,c}} \cdot \gamma_{\mathrm{sh,\alpha}} \quad (22)$$

where:

$\gamma_{\mathrm{sh,tc}}$ – coefficient accounting for the duration of curing,

$\gamma_{\mathrm{sh,RH}}$ – coefficient accounting for the ambient relative humidity,

$\gamma_{\mathrm{sh,vs}}$ – effective specimen size coefficient,

$\gamma_{\mathrm{sh,s}}$ – coefficient accounting for the concrete consistency,

$\gamma_{\mathrm{sh,\psi}}$ – coefficient accounting for the percentage content of fine aggregate in the total aggregate,

$\gamma_{\mathrm{sh,c}}$ – coefficient accounting for the cement content in the mix,

$\gamma_{\mathrm{sh,\alpha}}$ – coefficient accounting for the air entrainment of the mix.

In this study, the coefficients for the nonlinear concrete shrinkage models were estimated based on measurements of total and autogenous shrinkage. The estimation was performed using Matlab (Curve Fitting Toolbox) with the Levenberg-Marquardt method. This method is a hybrid of the Gauss-Newton and steepest descent methods.

2.3. Regression Model

The model fitting procedure operates iteratively using a nonlinear least squares method:

- it computes the model function values for the current parameters,
- calculates the fitting error,
- adjusts the parameters to minimize this error.

As a stopping criterion, the procedure terminates when either the change in parameter values or the objective function is less than 10^{-3}, or when the maximum number of iterations, set to 100, is reached. Physically meaningful constraints were applied to the estimated parameters (e.g., non-negative time constants), and the search space was restricted to a maximum of 15 times the nominal parameter values.

For the equation describing drying shrinkage in EC2 model, two coefficients were adopted for estimation. In Eq. (3) and (5), the following coefficients were introduced for estimation: ***b1*** and ***b2***. Additionally, in Eq. (7) and (8), which describe autogenous shrinkage, two coefficients were adopted for estimation: ***b3***, and ***b4***.

$$\varepsilon_{\mathrm{cd,0}} = \boldsymbol{b1} \cdot (220 + 110 \cdot \alpha_{\mathrm{ds1}}) \cdot exp\left(-\alpha_{\mathrm{ds2}} \cdot \frac{f_{\mathrm{cm}}}{f_{\mathrm{cm0}}}\right) \cdot \beta_{\mathrm{RH}} \cdot 10^{-6} \quad (3b)$$

$$\beta_{\mathrm{ds}}(t,t_{\mathrm{s}}) = \frac{(t-t_{\mathrm{s}})}{t-t_{\mathrm{s}}+\boldsymbol{b2}h_0{}^{1.5}} \quad (5b)$$

$$\varepsilon_{\mathrm{ca}}(\infty) = \boldsymbol{b3} \cdot (f_{\mathrm{ck}} - 10) \cdot 10^{-6} \quad (7b)$$

$$\beta_{\mathrm{as}}(t) = 1 - exp(-\boldsymbol{b4} \cdot t^{0.5}) \quad (8b)$$

The coefficients ***b1*** and ***b3*** define the nominal value for drying and autogenous shrinkage, respectively. Meanwhile, ***b2*** and ***b4*** shape the shrinkage progression as a function of time.

For the RILEM B4 model, four coefficients were adopted for estimation. In Eq. (11) which describe drying shrinkage, two coefficients were estimated: ***c1*** and ***c2***. Additionally, in Eq. (17), which describe autogenous shrinkage, two coefficients were estimated: ***c3***, and ***c4***.

$$\epsilon_{\mathrm{sh}}(t,t_0) = \boldsymbol{c1} \cdot tanh\left(\frac{t-t_0}{\boldsymbol{c2}}\right)^{0.5} \quad (23b)$$

$$c1 = \epsilon_{\mathrm{sh},\infty}(t_0) \cdot k_{\mathrm{h}}$$

$$c2 = \tau_{\mathrm{sh}}$$

$$\epsilon_{\mathrm{au}}(t,t_0) = \boldsymbol{c3} \cdot \left[1 + \left(\frac{\boldsymbol{c4}}{t+t_0}\right)^{\alpha}\right]^{r_{\mathrm{t}}} \quad (24b)$$

$$c3 = \epsilon_{\mathrm{au}\infty}$$

$$c4 = \tau_{\mathrm{au}}$$

For the ACI model, two coefficients were adopted for estimation. In Eq. (19), which describe total shrinkage, the coefficients estimated were: ***d1*** and ***d2***.

$$\varepsilon_{\mathrm{sh}}(t,t_{\mathrm{c}}) = \frac{(t-t_{\mathrm{c}})^{\alpha}}{\boldsymbol{d1}+(t-t_{\mathrm{c}})^{\alpha}} \cdot \boldsymbol{d2} \quad (25b)$$

$$d1 = f$$

$$d2 = \varepsilon_{\mathrm{shu}}$$

After performing the estimation, the quality of the model fit to the measurement data was evaluated based on the coefficient of determination, R^2:

$$R^2 = 1 - \frac{\sum(\varepsilon_{cs}(t_i)_m - \varepsilon_{cs}(t_i)_{reg})^2}{\sum(\varepsilon_{cs}(t_i)_m - \overline{\varepsilon_{cs}}(t_i)_m)^2} \quad (23)$$

where:
$\varepsilon_{cs}(t_i)_m$ – total shrinkage values obtained from measurements for successive times t_i,
$\overline{\varepsilon_{cs}}(t_i)_m$ – average total shrinkage value for the measurements,
$\varepsilon_{cs}(t_i)_{reg}$ – total shrinkage values obtained from the regression model for times t_i.

3. Results

3.1. Shrinkage measurement and concrete properties

As a control test, shrinkage measurements were conducted using the linear shrinkage test (LST), based on the EN 12390-16 [24] method, which serves as the basis for the currently applicable standardized measurement procedures. Traditionally cast specimens with dimensions of 40×40×160 mm were used in the test. The testing setup and the corresponding results are presented in Fig. 4, which shows three prediction models along with the LST results labeled as "Standard". The measurement of total shrinkage (TS) of 3D-printed samples was conducted continuously for 7 days, starting approximately 40 min after mixing with water. The results are presented in Fig. 5 (left). Independently, autogenous shrinkage (AS) measurements were performed; for this purpose, the sample was isolated to minimize evaporation. However, since it was necessary to install measurement points and avoid deforming the plastic samples, perfect isolation was impossible. This effect can be observed in Fig. 5 (right) between the 6th and 12th hour of measurement, where deformation stabilized due to the condensation of evaporated water. All samples for shrinkage measurements were placed in one laboratory under ambient conditions of T = 20 °C and RH = 35%.The figure highlights the rapid development of shrinkage within the first 24 h, which is not captured by standard shrinkage measurement methods.

The mean and characteristic compressive strength were also measured to determine all necessary parameters for the shrinkage estimation model. Cylindrical specimens with a diameter of 150 mm and a height of 300 mm were used for

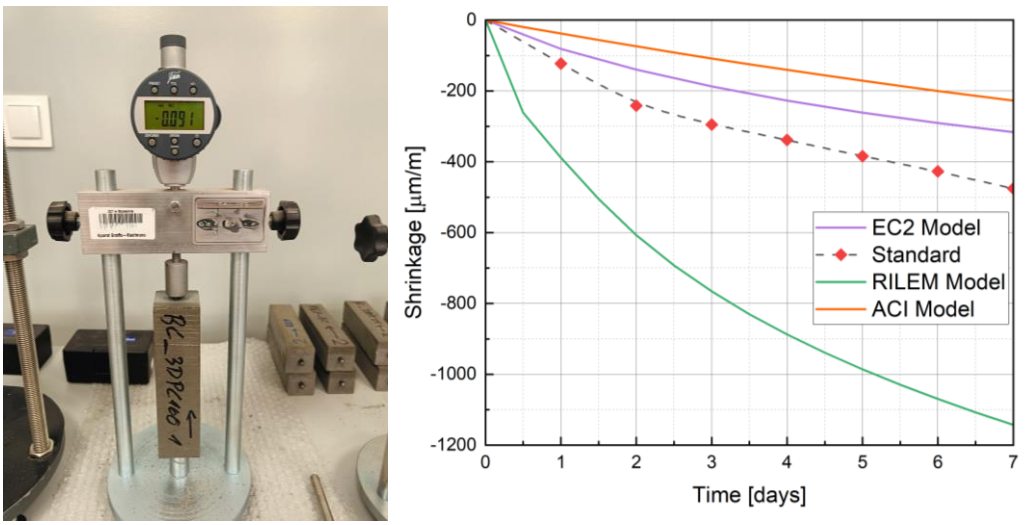

Fig. 4. Standard linear shrinkage test (LST): measuring setup (left); shrinkage evolution and comparison with model predictions (right).

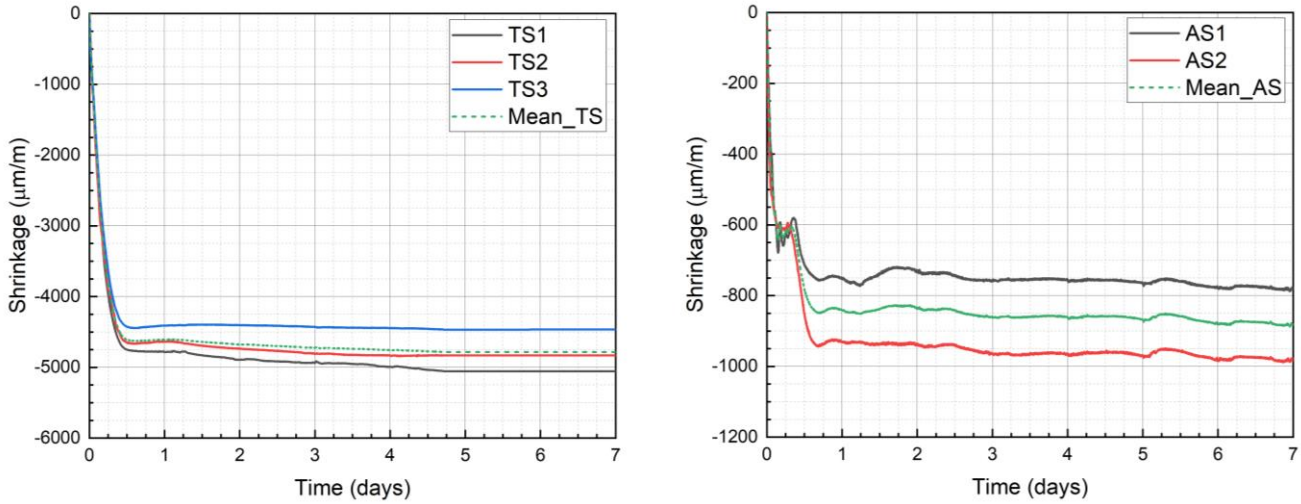

Fig. 5. Shrinkage measurement of 3D printed samples under ambient laboratory conditions (T = 20 °C; RH = 35%): total shrinkage—TS (left); autogenous shrinkage—AS (right).

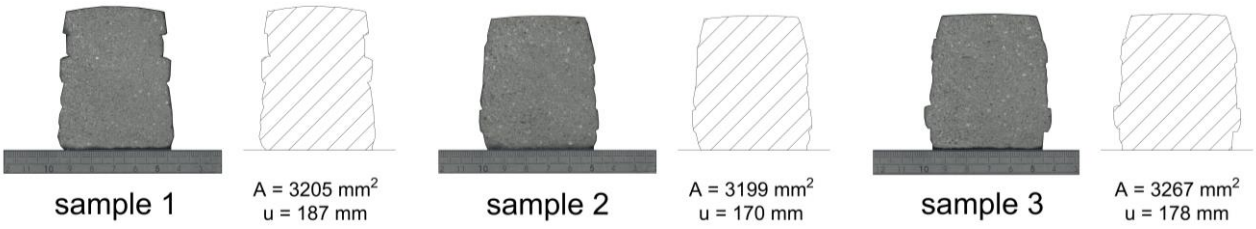

Fig. 6. Cross-section of the printed specimen after testing and definition of the exposed perimeter and area used to determine the characteristic cross-sectional dimension.

this purpose. The tested concrete exhibited a mean compressive strength of f_{cm} = 53 MPa after 28 days and a characteristic compressive strength of f_{ck} = 45 MPa, classifying it as C45/55 concrete. The modulus of elasticity, determined on 150×300 mm cylindrical specimens after 28 days, was 32.3 GPa. The characteristic cross section was determined based on Fig. 6, which illustrates the cut specimens after testing, with markings of their cross-sectional area and perimeter exposed to drying.

3.2. Shrinkage Prediction Model Fit

The estimated coefficient values for the EC2 model are presented in Table 2. The table includes the coefficient names and their values, the 95% confidence interval limits, standard deviations (σ) and Student's t statistics (t_{stat}). The *p*-values for the test verifying the significance of the coefficients in all the equations were below 0.05. Similarly, **TABLE 3** and **TABLE 4** present the estimation results for the RILEM and ACI models, respectively.

TABLE 2 Estimated coefficient values for EC2 model.

Coefficient	Mean	Confidence interval 95%		σ	tstat
		Lower	Upper		
b1	6.16	5.66	6.66	0.25	24.21
b2	0.0004	0.0003	0.0005	0.0001	7.90
b3	11.75	2.60	20.89	4.65	2.53
b4	3.93	0.47	7.40	1.76	2.23

TABLE 3 Estimated coefficient values for RILEM model.

Coefficient	Mean	Confidence interval 95%		σ	tstat
		Lower	Upper		
c1	3850.4	3240.7	4460.1	309.97	12.42
c2	0.21	0.130	0.281	0.038	5.36
c3	899.99	295.57	1504.4	307.28	2.93
c4	0.054	0.012	0.097	0.022	2.52

TABLE 4 Estimated coefficient values for ACI model.

Coefficient	Mean	Confidence interval 95%		σ	tstat
		Lower	Upper		
d1	0.083	0.082	0.083	3.26e-05	2529.62
d2	-4903.4	-4932.4	-4874.5	14.72	-333.11

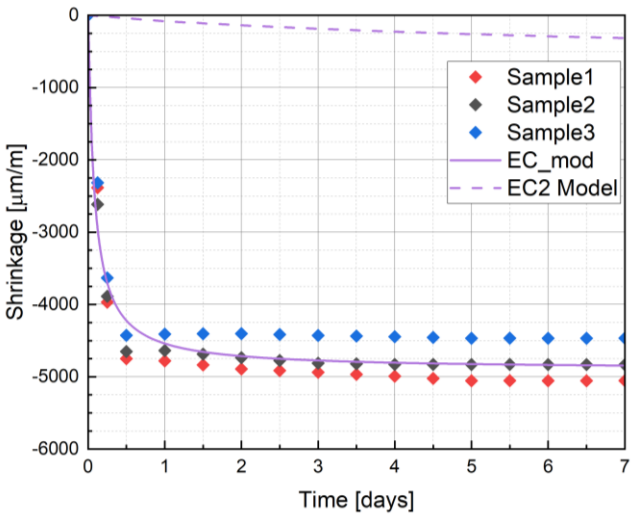

Fig. 7. Total shrinkage of 3D-printed concrete: measured data (markers) vs EC2 prediction (dashed) and recalibrated EC2 prediction (solid).

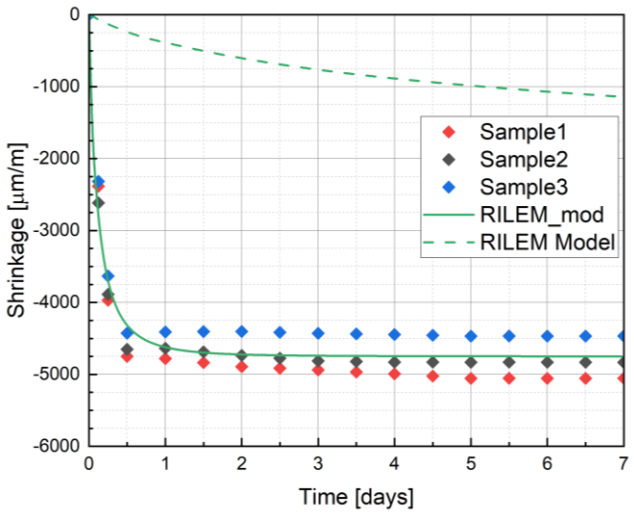

Fig. 8. Total shrinkage of 3D-printed concrete: measured data (markers) vs RILEM B4 prediction (dashed) and recalibrated RILEM B4 prediction (solid).

The *p*-values for all coefficients are lower than the significance level α = 0.05 indicating that all coefficients are statistically significant. The predicted total shrinkage, determined based on the estimated parameters, is compared with the measurement data in Fig. 7 to Fig. 9. The coefficients of determination (R^2) are 0.9435, 0.9662, and 0.9447 for the

EC2, RILEM, and ACI models, respectively, indicating an excellent fit of each model to the experimental data.

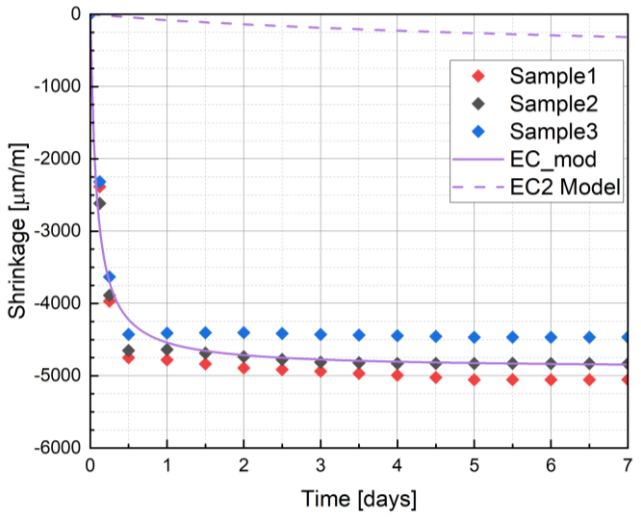

Fig. 9. Total shrinkage of 3D-printed concrete: measured data (markers) vs ACI 209-92 prediction (dashed) and recalibrated ACI 209-92 prediction (solid).

4. Discussion and conclusions

The measurements and analyses indicate the feasibility of adapting the models for predicting shrinkage, as outlined in Eurocode 2, RILEM recommendation or ACI 209-92, to the specific characteristics of 3D-printed concrete. The coefficients of determination (R^2) of around 0.94 demonstrate that modifying the coefficients (**TABLE 5**) developed for conventional concrete can achieve very high prediction accuracy. A key aspect is the adjustment of the shrinkage measurement methodology for printed elements, as standard methods such as the LST approach fail to capture the most critical changes occurring during the hardening process of 3D-printed concrete within the first 24 hours.

TABLE 5 Comparison of the models' coefficients and their estimated values.

EC2		b1	b2	b3	b4
	Model	0.85	0.04	2.5	0.2
	Estimation	6.16	0.0004	11.75	3.93
RILEM B4		c1	c2	c3	c4
	Model	-1657	20.32	-214.9	0.78
	Estimation	-3850.4	0.206	-899.99	0.055
ACI		d1	d2		
	Model	33.61	-1321		
	Estimation	0.083	-4903.4		

The coefficient estimation process for all three models demonstrated the necessity of modifying the function coefficients governing the time-dependent development of drying shrinkage (coef. b2, b4, c2, c4 and d1) and its nominal value, $\varepsilon_{cd,0}$ (b1, c1). It aligns with observations in the literature, as numerous studies (e.g. Ma et al. [19]) highlight significant differences in shrinkage deformations between printable and conventional concretes. Similarly, for autogenous shrinkage, the nominal value $\varepsilon_{ca}(\infty)$ (coef. b3 and c3) required estimation. It is expected to result primarily from the different binder compositions in 3D-printed concrete compared to traditional concretes as mentioned by Zhang et. al. [25].

When analyzing changes in model parameters, attention should be paid to their physical significance. In the case of the EC2 model, coefficient b1 determines the final value of drying shrinkage. For 3D-printed concrete, many researchers have emphasized that the absence of traditional formwork leads to significantly higher evaporation rates - an effect also confirmed by parameter estimation [19,26–28]. The value of b1 had to be increased several times, which reflects the accelerated moisture loss in printed elements.

On the other hand, a significant reduction in coefficient b2 can be interpreted as a necessary adjustment to the rate at which drying-induced shrinkage strains develop. The majority of these deformations occur within the first 24 hours of curing, which makes the impact of any model modification particularly noticeable. Future developments may require introducing additional coefficients that describe the evolution rate of shrinkage or more substantial revisions to the existing equation (Eq. 5). However, such changes would require a broader and more diverse experimental dataset.

Quantitatively, the early-age shrinkage magnitudes reported in the literature underscore the rapid kinetics addressed by the recalibrations. DIC- and optical-sensor-based studies reported free shrinkage of approximately 2400 µm/m within 3 h [10], 1500 µm/m after 24 h and ~3500 µm/m after 5 days [11], and up to 4000 µm/m after 3 h under non-curing conditions [12]. Markin and Mechtcherine reported values exceeding −9000 µm/m within 3 h [13]. In contrast, standardized measurements on cast specimens typically report markedly lower 28-day values (e.g., ~1600 µm/m in EN 12617-4-based testing [15] and >700 µm/m in Le et al. [17]), highlighting the strong dependence of measured shrinkage on method, geometry, and exposure.

The authors of the EC2 model also recommend limiting model calibration to no more than two parameters: one controlling the final shrinkage value, and the other modifying its time-dependent evolution. This same approach was applied when modifying the autogenous shrinkage component. As previously mentioned, 3D-printed concrete differs significantly from conventional structural concrete in terms of mix proportions—particularly binder content and water-to-cement ratio [29–32]. Increased binder content combined with reduced mixing water results in substantially higher autogenous shrinkage and altered kinetics, as confirmed by the estimated b3 and b4 coefficients.

A similar interpretation applies to the B4 model, which—like EC2—separately accounts for drying and autogenous shrinkage. The main difference lies in the role of coefficients c2 and c4, representing shrinkage half-times. As shown in Fig. 5, for 3D-printed elements this threshold is reached within the first 8–12 hours after printing. Coefficients c1 and c3, which define the ultimate shrinkage magnitude, are affected similarly to EC2: the absence of formwork and high binder content necessitate adjustments to the nominal values.

In contrast, the ACI model does not distinguish between shrinkage components and instead estimates total shrinkage as a single value. This makes it more difficult to isolate the impact of individual parameters. In this study, attention was focused on the final shrinkage value and the geometry-related coefficient. Since d1 appears in the denominator, reducing its value increases predicted shrinkage— reflecting the pronounced effect of drying surface exposure. For 3D-printed elements, the drying surface is much larger due to lack of formwork and slender geometries (40–50 mm print paths) [15,19]. Because key applicability assumptions of ACI 209-92 are violated, the recalibrated coefficients should be considered case-specific.

However, it should be emphasized that the presented studies are preliminary and primarily assess the applicability of baseline formulations for additively manufactured concrete. The calibration is based on a single mixture, geometry, and ambient condition (T = 20 °C, RH = 35%), with measurements up to 7 days. To achieve repeatable and universal solutions, a comprehensive database covering different geometries, compositions, and environmental conditions is required. Accordingly, further tests and supporting calculations are necessary to generalize the recommended coefficient sets and define their range of applicability.

ACKNOWLEDGEMENTS

This research was funded in whole by the National Science Centre, Poland within Project No. 2022/45/N/ST8/01277 (PRELUDIUM-21).

REFERENCES

1. Buswell et al. 3D Printing Using Concrete Extrusion: A Roadmap for Research. *Cem. Concr. Res.* **2018**, *112*, 37–49. https://doi.org/10.1016/j.cemconres.2018.05.006.
2. Wang et al. Interlayer Reinforcement of 3D Printed Concrete by the In-Process Deposition of U-Nails. *Cem. Concr. Res.* **2021**, *148*, 106535. https://doi.org/10.1016/j.cemconres.2021.106535.
3. Moelich et al. Modelling the Interlayer Bond Strength of 3D Printed Concrete with Surface Moisture. *Cem. Concr. Res.* **2021**, *150*, 106559. https://doi.org/10.1016/j.cemconres.2021.106559.
4. van den Heever et al. Evaluating the Effects of Porosity on the Mechanical Properties of Extrusion-Based 3D Printed Concrete. *Cem. Concr. Res.* **2022**, *153*, 106695. https://doi.org/10.1016/j.cemconres.2021.106695.
5. Mechtcherine et al. A Roadmap for Quality Control of Hardening and Hardened Printed Concrete. *Cem. Concr. Res.* **2022**, *157*, 106800. https://doi.org/10.1016/j.cemconres.2022.106800.
6. Ghourchian et al. Modelling the Development of Capillary Pressure in Freshly 3D-Printed Concrete Elements. *Cem. Concr. Res.* **2021**, *145*, 106457. https://doi.org/10.1016/j.cemconres.2021.106457.
7. Menna et al. Opportunities and Challenges for Structural Engineering of Digitally Fabricated Concrete. *Cem. Concr. Res.* **2020**, *133*, 106079. https://doi.org/10.1016/j.cemconres.2020.106079.
8. Krause et al. Strategic Optimization of 3D-Concrete-Printing Using the Method of CONPrint3D®; 2018. https://doi.org/10.22260/ISARC2018/0002.
9. Federowicz et al. Low-Carbon Cementitious Composite Incorporated with Biochar and Recycled Fines Suitable for 3D Printing Applications: Hydration, Shrinkage and Early-Age Performance. *Fract. Struct. Integr.* **2024**, *19* (71), 91–107. https://doi.org/10.3221/IGF-ESIS.71.08.
10. Moelich et al. The Effect of Restrained Early Age Shrinkage on the Interlayer Bond and Durability of 3D Printed Concrete. *J. Build. Eng.* **2021**, *43*, 102857. https://doi.org/10.1016/j.jobe.2021.102857.
11. Van Der Putten et al. Early Age Shrinkage Phenomena of 3D Printed Cementitious Materials with Superabsorbent Polymers. *J. Build. Eng.* **2021**, *35*, 102059. https://doi.org/10.1016/j.jobe.2020.102059.
12. Zhang et al. Plastic Shrinkage and Cracking of 3D Printed Mortar with Recycled Sand. *Constr. Build. Mater.* **2021**, *302*, 124405. https://doi.org/10.1016/j.conbuildmat.2021.124405.
13. Markin et al. Quantification of Plastic Shrinkage and Plastic Shrinkage Cracking of the 3D Printable Concretes Using 2D Digital Image Correlation. *Cem. Concr. Compos.* **2023**, *139*, 105050. https://doi.org/10.1016/j.cemconcomp.2023.105050.
14. Zhang et al. Advanced Measurement Techniques for Plastic Shrinkage and Cracking in 3D-Printed Concrete Utilising Distributed Optical Fiber Sensor. *Addit. Manuf.* **2023**, *74*, 103722. https://doi.org/10.1016/j.addma.2023.103722.
15. Shahmirzadi et al. Shrinkage Behavior of Cementitious 3D Printing Materials: Effect of Temperature and Relative Humidity. *Cem. Concr. Compos.* **2021**, *124*, 104238. https://doi.org/10.1016/j.cemconcomp.2021.104238.
16. CEN. EN 12617-4:2002 Products and Systems for the Protection and Repair of Concrete Structures - Test Methods - Part 4: Determination of Shrinkage and Expansion. European Committee for Standardization: Brussels, Belgium 2002, p 14.
17. Le et al. Hardened Properties of High-Performance Printing Concrete. *Cem. Concr. Res.* **2012**, *42* (3), 558–66. https://doi.org/10.1016/j.cemconres.2011.12.003.
18. Federowicz. Wpływ Pielęgnacji Na Odkształcenia Skurczowe Kompozytów Cementowych Wykorzystywanych w Technologii Druku 3D = The Effect of Curing on Shrinkage Deformation of Cementitious Composites Used 3D Printing Technology. *Zachodniopom. Uniw. Technol. w Szczecinie* **2023**, No. Doctoral thesis, 254.
19. Ma et al. Water Loss and Shrinkage Prediction in 3D Printed Concrete with Varying w/c and Specimen Sizes. *Cem. Concr. Compos.* **2024**, *149*, 105523. https://doi.org/10.1016/j.cemconcomp.2024.105523.
20. CEN. Eurocode 2: Design of Concrete Structures, Part 1-1: General Rules and Rules for Buildings. European Committee for Standardization: Brussels, Belgium 2004, p 225.
21. RILEM TC-247-MDC. RILEM Draft Recommendation: TC-242-MDC Multi-Decade Creep and Shrinkage of Concrete: Material Model and Structural Analysis*. *Mater. Struct.* **2015**, *48* (4), 753–70. https://doi.org/10.1617/s11527-014-0485-2.
22. ACI Committee 209. ACI PRC-209-92: Prediction of Creep, Shrinkage, and Temperature Effects in Concrete Structures (Reapproved 2008). Michigan, USA 2002, p 47.
23. Sikora et al. Insight into the Microstructural and Durability Characteristics of 3D Printed Concrete: Cast versus Printed Specimens. *Case Stud. Constr. Mater.* **2022**, *17*, e01320. https://doi.org/10.1016/j.cscm.2022.e01320.
24. CEN. EN 12390-16:2019 Testing Hardened Concrete - Part 16: Determination of the Shrinkage of Concrete. European Committee for Standardization: Brussels, Belgium 2019, p 13.
25. Zhang et al. Mix Design Concepts for 3D Printable Concrete: A Review. *Cem. Concr. Compos.* **2021**, *122*, 104155. https://doi.org/10.1016/j.cemconcomp.2021.104155.
26. Moelich et al. A Plastic Shrinkage Cracking Risk Model for 3D Printed Concrete Exposed to Different Environments. *Cem. Concr. Compos.* **2022**, *130*, 104516. https://doi.org/10.1016/j.cemconcomp.2022.104516.
27. Markin et al. Specifics of Plastic Shrinkage in 3D-Printed Concrete Elements. *Cem. Concr. Res.* **2024**, *184*, 107512. https://doi.org/10.1016/j.cemconres.2024.107512.
28. Ma et al. Effect of Drying Environment on Mechanical Properties, Internal RH and Pore Structure of 3D Printed Concrete. *Constr. Build. Mater.* **2022**, *315*, 125731. https://doi.org/10.1016/j.conbuildmat.2021.125731.
29. Şahin et al. Assessment of Materials, Design Parameters and Some Properties of 3D Printing Concrete Mixtures; a State-of-the-Art Review. *Constr. Build. Mater.* **2022**, *316*, 125865. https://doi.org/10.1016/j.conbuildmat.2021.125865.
30. Rehman et al. 3D Concrete Printing: A Systematic Review of Rheology, Mix Designs, Mechanical, Microstructural, and Durability Characteristics. *Materials (Basel).* **2021**, *14* (14), 3800. https://doi.org/10.3390/ma14143800.
31. Dilawar Riaz et al. Inclusive Characterization of 3D Printed Concrete (3DPC) in Additive Manufacturing: A Detailed Review. *Constr. Build. Mater.* **2023**, *394*, 132229. https://doi.org/10.1016/j.conbuildmat.2023.132229.
32. Hou et al. A Review of 3D Printed Concrete: Performance Requirements, Testing Measurements and Mix Design. *Constr. Build. Mater.* **2021**, *273*, 121745. https://doi.org/10.1016/j.conbuildmat.2020.121745.